Drug Design, Development and Therapy

Dovepress
Taylor & Francis Group

Open Access Full Text Article

ORIGINAL RESEARCH

Mechanism of the Traditional Chinese Medicine Simiao Biejia Decoction Improves the Diabetes Mellitus-Induced Erectile Dysfunction in Rats

Yuanyuan Liu[1,*], Dalin Sun[2,*], Dong Xing[1], Yiqi Rui[3], Yihan Jin[4], Peng Wang[3], Bin Cai[2], Chuyu Li[5], Chao Gao[5], Yugui Cui[5], Baofang Jin[2]

[1]School of Medicine, Southeast University, Nanjing, Jiangsu, 210003, People's Republic of China; [2]Department of Integrative Medicine and Andrology, Zhongda Hospital, School of Medicine, Southeast University, Nanjing, Jiangsu, 210009, People's Republic of China; [3]Department of General Surgery, Jiangsu Province Official Hospital, Geriatrich Hospital of Nanjing Medical University, Nanjing, Jiangsu, 210024, People's Republic of China; [4]Reproductive Medicine Center, Zhongda Hospital, School of Medicine, Southeast University, Nanjing, Jiangsu, 210009, People's Republic of China; [5]State Key Laboratory of Reproductive Medicine and Offspring Health, Center of Clinical Reproductive Medicine, The First Affiliated Hospital of Nanjing Medical University, Nanjing, Jiangsu, 210006, People's Republic of China

*These authors contributed equally to this work

Correspondence: Yugui Cui State Key Laboratory of Reproductive Medicine and Offspring Health, Center of Clinical Reproductive Medicine, The First Affiliated Hospital of Nanjing Medical University, No. 368 Jiangdong North Road, Nanjing, Jiangsu, 210006, People's Republic of China, Email cuiygnj@njmu.edu.cn; Baofang Jin, Department of Integrative Medicine and Andrology, Zhongda Hospital, School of Medicine, Southeast University, No. 87 Dingjiaqiao, Gulou District, Nanjing, Jiangsu, 210009, People's Republic of China, Email hexiking@126.com

Objective: Simiao Biejia (SMBJ) granules, a traditional Chinese herbal remedy, have been used to treat erectile dysfunction caused by diabetes mellitus (DMED). However, the molecular mechanisms underlying SMBJ's therapeutic effects remain unclear. This study aimed to investigate the effects and mechanisms of SMBJ in a rat model of DMED using network pharmacology, proteomics, and molecular docking.

Methods: A rat model of DMED was established, and SMBJ granules were administered (0, 7.1, 14.2, and 28.4 mg/kg/d, respectively) for 4 weeks. Erectile function was evaluated by measuring intracavernous pressure and mean arterial pressure. The active compounds in SMBJ were analyzed by gas chromatography and identified using network pharmacology and bioinformatics. Potential targets in the penile tissue was identified via proteomics and validated by Western blotting. Molecular docking was used to assess the binding affinity between bioactive compounds and primary targets.

Results: SMBJ significantly improves erectile function and ameliorates DMED in rats by reducing corpus cavernosum fibrosis, decreasing eNOS and nNOS levels, alleviating oxidative stress in penile tissue, and mitigating damage to smooth muscle cells (SMCs) and vascular endothelial cells (VECs). Network pharmacology and proteomics identified 24 potential SMBJ targets in DMED. The 4 drug molecules identified were involved in the therapeutic effects of SMBJ, among which luteolin was predicted to be the core drug component. Luteolin bound directly with AKT1, a key differentially expressed protein in the penile tissue of DMED rats. Further analysis showed that luteolin in SMBJ activates the PI3K/Akt pathway and regulation of nNOS and NF-kB expression in the penile tissue of DMED rats to improve erectile function.

Conclusion: SMBJ improved oxidative stress damage, vascular endothelial repair, and angiogenesis in the penile tissue of DMED rats. Luteolin is one of the core drug components of SMBJ in DMED treatment that regulates PI3K/AKT-related pathways.

Keywords: luteolin, erectile dysfunction, diabetes, Simiao Biejia, network pharmacology

Introduction

Diabetes mellitus-induced erectile dysfunction (DMED) is a serious health problem that affects the lifestyle of people with diabetes. Experts predict that the number of ED patients will reach 322 million by 2025.[1] The global prevalence of DMED varies significantly by region, ranging from 35.8% to 86.1%,[2] with approximately 12% of diabetic patients

Received: 15 October 2024
Accepted: 18 March 2025
Published: 3 April 2025

Graphical Abstract

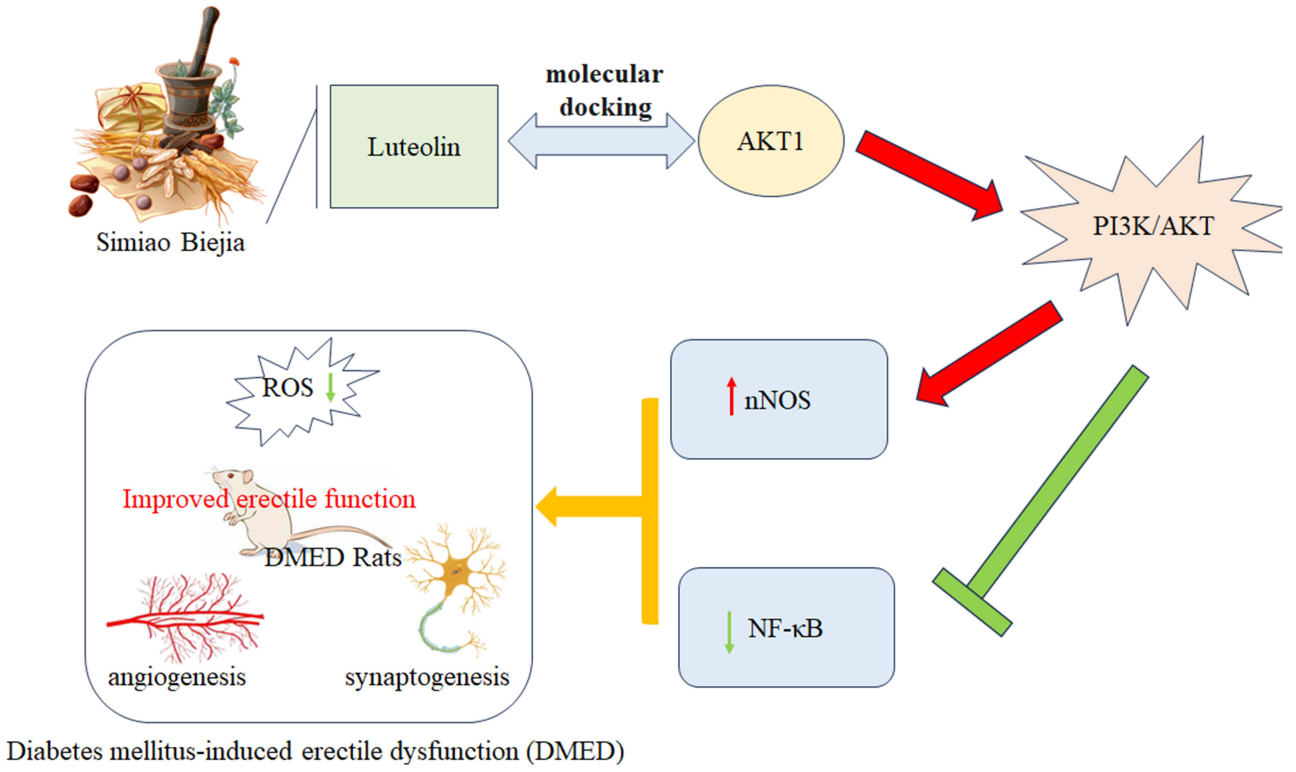

experiencing ED as an initial clinical manifestation.[3] However, the underlying molecular mechanisms remain unclear. Reactive oxygen species (ROS) play a critical role in the pathophysiology of DMED by disrupting endothelial function and contributing to vascular complications.[4] Chronic hyperglycemia induces excessive ROS production, leading to oxidative stress, which in turn reduces nitric oxide (NO) bioavailability and impairs vascular relaxation.[5] This oxidative imbalance also promotes inflammation, lipid peroxidation, and endothelial cell apoptosis, further exacerbating vascular dysfunction. The detrimental effects of ROS extend to key signaling pathways, such as PI3K/Akt,[6] resulting in endothelial damage and impaired angiogenesis. Oxidative stress damage can be evaluated by the levels of SOD and malondialdehyde (MDA). In DMED, the endothelial cell dysfunction-induced inhibition of smooth muscle relaxation and the replacement of smooth muscle cells (SMCs) with fibroblasts are two direct factors in erectile dysfunction (ED).[7,8] One of the DMED pathophysiological characteristics is the downregulated production of NO because of the dysfunction of vascular endothelial cells (VECs).[9] Three isoforms of nitric oxide synthase (NOS), namely neuronal NOS (nNOS), endothelial NOS (eNOS), and inducible NOS (iNOS), are responsible for the synthesis of NO. Insufficient cGMP secretion under low NO conditions inhibits smooth muscle relaxation in the penis, resulting in ED.[10] Furthermore, insufficient cavernous VEC repair and angiogenesis are other factors affecting DMED. Regarding the treatment of DMED, despite the promising outcomes of PDE5i in individuals with ED, the response rate of DMED is only 44%.[11] Notably, the therapeutic impact of PDE5i relies on the appropriate functioning of tissue effectors, including nerves, blood vessels, and cavernous tissues.[12] Therefore, restoring NOS and NO bioactivity, suppressing oxidative stress, promoting angiogenesis and cavernous endothelial cell repair represent promising strategies for DMED treatment, including traditional Chinese medicine.

The Simiao Biejia decoction (SMBJ) is derived from the combination and modification of two traditional Chinese medicines (TCMs) formulas: the Simiao Yongan Decoction (SMYA) and Erdi Biejia Decoction (EDBJ). By adjusting the composition and proportions of the herbal ingredients in these formulas, SMBJ has been developed to enhance

therapeutic efficacy. Previous studies have demonstrated its effectiveness in treating diabetic vascular complications and ED.[13–15] Ingredients include *Carapax trionycis, Radix salviae liguliobae, Radix angelicae sinensis, Radix glycyrrhizae, Radix puerariae, Rhizoma coptidis, Radix astragali, Flos lonicerae, Semen litchi, Radix rehmanniae preparata, Radix scrophulariae, Fructus lycii, and Epimrdii herba*. TCM provides a unique perspective on the pathogenesis and treatment of DMED. According to TCM principles, DMED is primarily associated with "yin deficiency and internal heat" and "qi stagnation and blood stasis".[8,16] These imbalances are believed to impair the meridians and hinder penile function, ultimately contributing to the development of DMED. Recent studies have demonstrated the efficacy of TCM-based therapies in DMED management. Herbal formulations such as SMBJ have been shown to reduce oxidative stress and improve endothelial function,[17] while acupuncture may help regulate qi flow and enhance penile hemodynamics.[18] SMBJ integrates the benefits of both prescriptions and exhibits properties of nourishing yin, clearing heat, regulating qi, and enriching blood. However, the key bioactive ingredients and targets of SMBJ for DMED remain unclear. Hence, this research aimed to explore the key objectives, pathways of communication, and biological processes of SMBJ in managing DMEM in a rat model with diabetes, utilizing a combination of network pharmacology, proteomics, and molecular docking. This is a novel approach to the clinical management of DMED and comprehensive investigation of active components in this TCM.

Materials and Methods

Experimental Animals and Drug Preparation

The GK rat model, a non-obese diabetic animal model of type 2 diabetes mellitus, has been extensively utilized in scientific studies, particularly in researching microvascular complications associated with diabetes. Wistar rats are homogeneous with them as a control. Forty male GK rats, with an average weight of 280–320 g and aged 14 weeks, along with 10 male Wistar rats of the same age, were acquired from the Animal Experiment Centre of Cavens in Changzhou, Jiangsu, China. Southeast University, China's Animal Experimental Ethical Inspection Committee approved all animal experiments (approval no: 20200402003), and laboratory animal welfare adheres to the Laboratory Animal—Guideline for Ethical Review of Animal Welfare (GB/T 35892-2018) promulgated jointly by the General Administration of Quality Supervision, Inspection and Quarantine of the People's Republic of China and the Standardization Administration of China. SMBJ Decoction consists of 13 Chinese herbal granules as detailed in Table 1. Specifically, it includes 3.3 grams of Carapax trionycis, 5 grams of Radix salviae liguliobae, 6.7 grams of Radix angelicae sinensis, 1.7 grams of Radix glycyrrhizae, 4 grams of Radix puerariae, 0.7 grams of Rhizoma coptidis, 4 grams of Radix astragali, 3.3 grams of Flos lonicerae, 3 grams of Semen litchi, 7.7 grams of Radix rehmanniae preparata, 6.6 grams of Radix

Table 1 Plant Names

Chinese Name	Latin Name	Raw Material Medicine Dose(g)	Granule(g)
DAN SHEN	*Radix Salviae liguliobae*	10	5.0
DANG GUI	*Radix Angelicae sinensis*	10	6.7
JIN YIN HUA	*Flos Lonicerae*	10	3.3
SHU DI HUANG	*Radix Rehmanniae Preparata*	10	7.7
XUAN SHEN	*Radix Scrophulariae*	10	6.6
LI ZHI HE	*Semen Litchi*	30	3.0
GE GEN	*Radix Puerariae*	10	4.0
HUANG LIAN	*Rhizoma Coptidis*	3	0.7
GAN CAO	*Radix Glycyrrhizae*	5	1.7
BIE JIA	*Carapax Trionycis*	20	3.3
YIN YANG HUO	NA	10	2.0
GOU QI ZI	*Fructus Lycii*	10	8.3
HUANG QI	*Radix Astragali*	20	4.0
			56.3

https://doi.org/10.2147/DDDT.S495366

scrophulariae, 8.3 grams of Fructus lycii, and 2 grams of Epimedii herba. These granules are supplied by the Pharmacy of Zhongda Hospital, Southeast University. These ingredients were finely ground and dissolved in deionised water to create various concentrations of SMBJ suspension. The suspension was subsequently stored at −80 °C. The suspensions were thoroughly mixed before the experiments.

Composition Analysis of SMBJ

In summary, a solution containing 100 μL of SMBJ was combined with 300 μL of 50% methanol, followed by agitation for 10 minutes and centrifugation at 20,000 rpm for 10 minutes at 4 degrees Celsius to isolate the supernatant for UHPLC-QTOF-MS analysis. Chromatographic separation was carried out using a column (AQ-C18, 150×2.1 mm, 1.8 μm, Welch) at a flow rate of 0.3 mL/min and a temperature of 35 °C, with an injection volume of 5 μL. The liquid component was a mixture of methanol and an aqueous solution containing 0.1% Formic acid with a gradient of B decreasing from 98% to 5% over different time intervals. Full mass/dd-MS2 was conducted under ESI positive and negative ion scanning modes with specific parameters including resolution, scan range, spray voltage, capillary temperature, collision gas purity, collision energy values, sheath gas, auxiliary gas, and data collection duration. Data from the high-resolution liquid mass was organized using Compound Discoverer 3.3 and cross-referenced with mzCloud. 689 compounds were matched on mzCloud, with 393 having a score >60 points.

Experimental Design

GK rats (n=40) were randomly divided into DMED (positive control), LSMBJ (low-dose), MSMBJ (medium-dose), and HSMBJ (high-dose) groups, with 10 rats per group. The normal control group included 10 Wistar rats. Rats in the LSMBJ (2.44g/kg, 3 times the human dosage), MSMBJ (4.88g/kg, 6 times the human dosage), and HSMBJ (9.76g/kg, 12 times the human dosage) groups were administered SMBJ via oral gavage. Rats in the DMED and control groups were administered saline via oral gavage twice daily. After 4 weeks of SMBJ treatment, erectile function was assessed in all rats. After sacrificing the rats, fresh penile tissue (<1.0 mm^3) was carefully isolated for transmission electron microscopy (TEM).[19] A section of the penile tissue was preserved overnight at 4 °C using tissue stationary liquid (G1101, Servicebio, China), dehydrated, embedded in paraffin, sliced into 5 m-thick sections, and placed on slides for additional examination. Quickly freeze the sample in liquid nitrogen and store it in a refrigerator at −80 ° C.

Evaluation of Erectile Function

Erectile function is closely related to the integrity of the cavernous nerve and the hemodynamic response of the corpus cavernosum. This experiment aims to assess the physiological response of erectile function by measuring intracavernous pressure (ICP) and mean arterial pressure (MAP), which are widely recognized indicators of erectile function in preclinical studies.

At the end of the drug administration, all rats were anaesthetised using 40 mg/kg of pentobarbital sodium (Sigma-Aldrich, Copenhagen, Denmark) via intraperitoneal injection. The cavernous nerve was exposed via a midline laparotomy. A 25-gauge needle, heparinised at 200 U/mL, was inserted into the penis to intubate the corpus cavernosum. It was then connected to a pressure sensor via polyethylene-50 tubing. Excitation was performed using a 5 V voltage at a frequency of 20 hz for 60 seconds. ICP and MAP were recorded by inserting a needle at the aortic bifurcation. Detect the values of maximum intracavernosal pressure (mICP) and area under the curve (AUA) and analyze the ratio to MAP.

Histological Assessment

The structural integrity of penile tissue is crucial for erectile function, which relies on a balanced composition of smooth muscle, connective tissue, and vascular structures. This experiment aims to evaluate morphological changes, tissue composition, and protein expression in penile tissues to understand the impact of the drug intervention on histological and molecular levels.

The penile tissue was promptly fixed at 4 °C overnight using tissue stationary liquid (G1101, Servicebio, China), dehydrated, embedded in paraffin, sliced into 5 m-thick sections, and placed on slides. Following dewaxing, the tissue underwent staining with haematoxylin and eosin (H&E; G1104; Wuhan Servicebio Technology Co., Ltd., Wuhan, China)

and Masson's stain (G1006; Wuhan Servicebio Technology Co., Ltd.) to evaluate histology. The immunohistochemical analysis utilized primary antibodies including rabbit anti-collagen I (1:200, ab16667, Abcam), rabbit anti-collagen IV (1:200, ab16667, Abcam), mouse anti-eNOS (1:200, GB12086-100, Servicebio), rabbit anti-nNOS (1:200, GB11145-100, Servicebio), and rabbit anti-smooth muscle actin (SMA) (1:200, 14395-1-AP, Proteintech). Nikon microscope in Tokyo, Japan was used to capture microscopic pictures.

Enzyme-Linked Immunosorbent Assay (ELISA) for cGMP, NO, SOD, and MDA

The biochemical markers cGMP, NO, SOD, and MDA are critical for evaluating oxidative stress, endothelial function, and nitric oxide signaling, which are key mechanisms in the regulation of erectile function. This experiment aims to quantify these markers to understand the biochemical effects of the drug intervention and their potential role in restoring or improving erectile function.

In short, the penile tissue was homogenized and centrifuged in a glass Teflon homogenizer with pre-cooled physiological saline at 3000 × g for 15 minutes at 4 °C. Subsequently, the tissue was broken down with a tissue lysate solution. The levels of NO, SOD, cGMP, and MDA in the supernatant were measured using ELISA kits from different manufacturers, following the provided instructions.

Proteomics Analysis of Rat Penile Tissue

Proteomics analysis provides a comprehensive understanding of the protein expression profile and molecular pathways involved in physiological and pathological conditions. This experiment aims to identify changes in protein expression and post-translational modifications in penile tissue following drug intervention, offering insights into the underlying mechanisms that regulate erectile function and tissue remodeling.

Penile tissue was quickly homogenized two times in SDT buffer using an MP Fastprep-24 automated homogenizer with quartz sand in 2 mL tubes (6.0 M/S, 30s, twice). The tissue homogenates were ultrasonic and boiled for 10 min, followed by centrifugation at a speed of 14000 × g for 30 min. After filtration through 0.22 μm filters, the protein concentration of the filtrate was measured with the BCA Protein Assay Kit (P0012, Beyotime). Subsequently, protein extraction was performed using FASP enzymatic hydrolysis. Subsequently, 20 grams of protein from each specimen were combined with a fivefold excess of loading buffer, then subjected to a 5-minute heating process, and subsequently separated using a 12% sodium dodecyl sulfate-polyacrylamide gel. Coomassie Blue R-250 staining was utilized for visualization of the protein bands. Samples containing 100 grams of proteins underwent reduction using 100 mm of DTT at 99 °C for 6 minutes. After this step, the detergent, DTT, and various small compounds were eliminated through ultrafiltration (Sartorius, 30 kD) with UA buffer (8 M urea, 150 mm Tris-HCl, pH 8.5). Next, 100 μL of iodoacetamide solution was added to block cysteine residues and incubated for 30 minutes. The filters were then rinsed with UA buffer and NH4HCO3 buffer. The protein mixtures were digested with trypsin overnight at 37 °C. Peptides were collected and desalted using a C18 column. Peptide content was estimated using UV light. Peptide content was determined at 0.1% g/L using a UV light at 280 nm with an extinction coefficient of 1.1, based on vertebrate proteins (tyrosine and tryptophan).

The Bruker timsTOF Pro from Bremen, Germany was used in PASEF mode with specific settings: mass range 100–1700 m/z, 1/K0 from 0.75 to 1.4 V·s/cm2, ramp time 100 ms, capillary voltage 1500 V, dry gas flow 3 L/min, dry temperature 180 °C. PASEF configuration included 10 MS/MS scans lasting 1.16 seconds, covering charges 0–5, excluding 10/13 ions for 0.5 minutes, aiming for intensity of 10000 with threshold of 2500, and using CID collision energy be.

Peptide segments were identified using the PaSER2023 database search library software, while protein quantification was conducted with the Uniport database (http://www.UniProt.org).

Network Pharmacology Analysis

Network pharmacology is an integrative approach that connects active compounds, target genes, and disease-related pathways to elucidate the mechanisms of multi-component, multi-target therapeutics. This analysis aims to identify the molecular targets and biological pathways through which SMBJ (a traditional herbal remedy) may exert therapeutic effects on DMED, providing a systematic understanding of its pharmacological mechanisms.

The active components of the herbal remedies in SMBJ were obtained from the HERB database (http://herb.ac.cn/).[20] Notably, the targets (human proteins) of various drugs can also be annotated on the HERB database. To further screen targets specifically associated with DMED, target genes associated with type 2 diabetes and ED dysfunction were screened using the HERB database and annotated using the Comparative Toxicology Database (CTD; association score > 20; https://ctdbaseorg/).[21] HomoloGene annotates homologous gene relationships between humans and rats.[22] Furthermore, the Venny package was utilized to discover overlapping targets in the Venn diagram of SMBJ active compounds related to both ED and type 2 diabetes (https//bioinfogp.cnb.csic.es/tools/venny/index.html). Possible targets for SMBJ in DMED may involve these shared targets.

The core targets were identified by creating a protein-protein interaction (PPI) network that integrated compounds, targets, and disease-related targets from the STRING database (https//string-db.org/), which was then analyzed using Cytoscape 3.9.1 software with the CytoHubba plugin. Subsequently, potential targets of SMBJ in DMED were identified. The association between target genes and diseases (based on rat phenotype and human disease gene relationship databases) was analysed using the ToppGene toolkit.[23] Furthermore, an analysis of KEGG pathways was conducted to discover pathways significantly associated with DMED due to the treatment, using a statistical enrichment threshold of FDR < 0.05.

Western Blot

Western blot is a widely used technique to detect and quantify specific proteins in biological samples, providing insights into their expression levels, activation states, and involvement in signaling pathways. This experiment aims to evaluate the expression and phosphorylation of key signaling molecules and markers related to endothelial function, smooth muscle integrity, fibrosis, and angiogenesis in cavernous tissue. These findings will help elucidate the molecular mechanisms underlying the effects of the drug intervention on DMED.

The Protein Ladder (10~250 kDa, Cat.No. WJ103) was purchased in Shanghai Yamay Biomedical Technology Co., Ltd. Protein was extracted from cavernous tissue using the RIPA kit, and its concentration was determined with the BCA Protein Assay Kit. Equivalent amounts of protein were isolated, transferred to membranes, and incubated with primary antibodies overnight at 4 °C: Mouse anti-p-AKT1 (1:10000, 66444-1-Ig, Proteintech), rabbit anti-AKT1 (1:5000, 10176-2-AP, Proteintech), rabbit anti-PI3K (1:500, 20584-1-AP, Proteintech), mouse anti-NF-kB (1:1000, 66535-1-Ig, Proteintech), mouse anti-p-Mtor (1:5000, 67778-1-Ig, Proteintech), rabbit anti-mTOR(1:5000, 28273-1-AP, Proteintech), rabbit anti-SMA (1:5000, 14395-1-AP, Proteintech), rabbit anti-Notch3(1:1000, 55114-1-AP, Proteintech), rabbit anti-PTPN12 (1:2000, 31215-1-AP, Proteintech), rabbit anti-YAP1 (1:5000, 13584-1-AP, Proteintech), rabbit anti-ANG1(1:5000, 23302-1-AP, Proteintech), rabbit anti-nNOS (1:1000, ab5589, Abcam), rabbit anti-VEGF (1:5000, 19003-1-AP, Proteintech), rabbit anti-CBPA1(1:5000, ab109252, Abcam), rabbit anti-ASNS (1:5000, 16481-1-AP, Proteintech), rabbit anti-β-actin (1:5000, 20536-1-AP, Proteintech). After washing, the membranes were incubated with horseradish peroxidase-conjugated goat anti-rabbit IgG (1:5000, SA00001-2; Proteintech) and horseradish peroxidase-conjugated goat anti-mouse IgG (1:5000, SA00001-1; Proteintech). Finally, the antibody reaction was visualised using a detection kit and quantified using ImageJ software.

Molecular Docking

Molecular docking is a computational approach used to predict the binding affinity and interaction patterns between small molecules (ligands) and biological targets (proteins). This experiment aims to evaluate the potential of active components in SMBJ to bind key targets, such as AKT1, and to understand the molecular basis of their pharmacological effects on DMED. By analyzing binding free energy and non-covalent interactions, the study provides insights into the strength and specificity of these interactions, aiding in the identification of key therapeutic compounds.

To assess the ability of the active components to bind to the anticipated targets, fully automated blind molecular docking with the high-throughput virtual molecule screening software InstaDock (https://hassanlab.org/instadock/). Docking validation was performed using CB-Dock (https://cadd.labshare.cn/cb-dock2/php/index.php) sorted according to the binding free energy comprehensive score.[16] The chemical structures of the active ingredients were obtained from PubChem (https://pubchem.ncbi.nlm.nih.gov/). The 3D configuration of AKT1 was acquired from the Protein Data Bank

(PDB) database (http://www.rcsb.org/) (PDB ID 6S9W). Drug-binding pockets in humans and rats were predicted using the CurPocket method in the CB-Dock.[24,25] Non-covalent interactions between the proteins and their ligands were identified using the tool of protein-ligand interaction profiler (https://plip-tool.biotec.tu-dresden.de/plip-web/plip/index).[26]

Statistical Analysis

Statistical analysis was conducted using GraphPad Prism version 9.5 for Windows (GraphPad Software, La Jolla, CA, USA). Data are expressed as the mean ± standard deviation (SD) or standard error (SE) where appropriate to illustrate variability. A post-hoc test was performed subsequent to a one-way ANOVA to identify significant differences within normally distributed data. Statistical significance was established at a p-value of less than 0.05. To ensure the reliability of the results, appropriate statistical methods were applied to assess and control individual variability.

Results

Screening for the Active Compounds of SMBJ

The total ion chromatogram of SMBJ was obtained through UHPLC-QTOF-MS analysis, and compounds were qualitatively identified using Compound Discoverer 3.3 software. As shown in Figure 1, 33 compounds were identified in positive ion mode, while 13 compounds were identified in negative ion mode, as listed in Table 2 and Table 3.

SMBJ Improves Erectile Function in Rats With DMED

The body weight, blood glucose levels, and testosterone levels of the rats with diabetes at the conclusion of the experiment are depicted in Figure 2A. A notable increase in blood glucose levels was observed in the DMED group compared to the control group, which was subsequently reversed following intervention with SMBJ (Figure 2B). Additionally, the decreased testosterone levels in DMED rats were significantly improved in rats treated with SMBJ (Figure 2C). Otherwise, in order to examine the impact of SMBJ on erectile function with DMED, a rat model of DMED

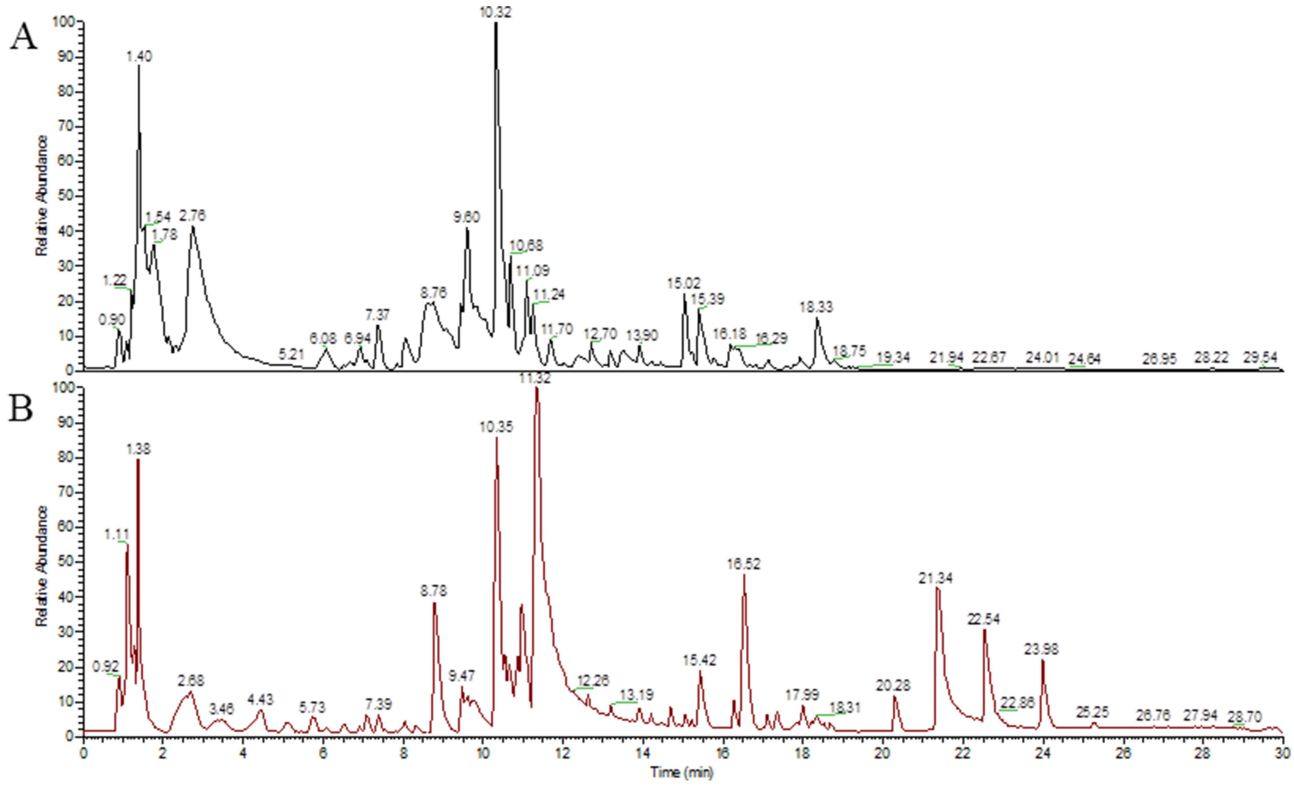

Figure 1 UHPLC-QTOF-MS analysis of SMBJ. (**A**) Negative ion chromatography. (**B**) Positive ion chromatography.

https://doi.org/10.2147/DDDT.S495366

Table 2 High Resolution Mass Spectrometry Data and Elemental Composition of LCG (Positive Ion Mode)

No.	Name	Formula	MW	m/z	RT (min)	Ionization	Area
1	Adenosine	$C_{10}H_{13}N_5O_4$	267.0965	268.10376	4.447	[M+H]+1	3950705347
2	3-{[(2S,3R,4S,5S,6R)-6-({[(2R,3R,4R)-3,4-dihydroxy-4-(hydroxymethyl)oxolan-2-yl]oxy}methyl)-3,4,5-trihydroxyoxan-2-yl]oxy}-2-methyl-4H-pyran-4-one	$C_{17}H_{24}O_{12}$	420.12654	421.13382	7.223	[M+H]+1	178785945.8
3	D-(+)-Proline	$C_5H_9NO_2$	115.06355	116.07083	1.385	[M+H]+1	8836086502
4	Dipropyleneglycol dibenzoate	$C_{20}H_{22}O_5$	342.14616	343.15347	17.998	[M+H]+1	1053825263
5	2-(8-Hydroxy-4a,8-dimethyldecahydro-2-naphthalenyl)acrylic acid	$C_{15}H_{24}O_3$	234.16177	235.1691	17.729	[M+H]+1	208489396.9
6	(2S,3R,4S,5S,6R)-2-({4a,5,7-trihydroxy-7-methyl-1H,4aH,5H,6H,7H,7aH-cyclopenta[c]pyran-1-yl}oxy)-6-(hydroxymethyl)oxane-3,4,5-triol	$C_{15}H_{24}O_{10}$	381.16304	382.17032	7.393	[M+H]+1	1110456359
7	Dihexyl nonanedioate	$C_{21}H_{40}O_4$	263.22481	264.23209	12.488	[M+H]+1	145708905.8
8	(1S,3R,4S,5R)-3,5-bis({[(2E)-3-(3,4-dihydroxyphenyl)prop-2-enoyl]oxy})-1,4-dihydroxycyclohexane-1-carboxylic acid	$C_{25}H_{24}O_{12}$	516.1267	517.13397	14.127	[M+H]+1	331872765.8
9	Genistin	$C_{21}H_{20}O_{10}$	432.10532	433.11258	12.037	[M+H]+1	395512803
10	L-Isoleucine	$C_6H_{13}NO_2$	131.09467	132.10194	2.49	[M+H]+1	2864202713
11	Trigonelline	$C_7H_7NO_2$	137.04759	138.05487	1.432	[M+H]+1	1276378547
12	Di(2-ethylhexyl) phthalate	$C_{24}H_{38}O_4$	390.27618	391.28345	22.847	[M+H]+1	328946563.2
13	Dibutyl phthalate	$C_{16}H_{22}O_4$	278.15149	279.15878	18.337	[M+H]+1	4470385069
14	Nicotinic acid	$C_6H_5NO_2$	123.03231	124.03959	2.112	[M+H]+1	383948641.6
15	Ononin	$C_{22}H_{22}O_9$	430.12584	431.13312	13.212	[M+H]+1	1340136527
16	Cynaroside	$C_{21}H_{20}O_{11}$	448.10025	449.10742	12.628	[M+H]+1	215761547.6
17	L-Histidine	$C_6H_9N_3O_2$	155.06948	156.07677	1.127	[M+H]+1	130393412.9
18	Ononin	$C_{22}H_{22}O_9$	430.12603	431.1333	13.637	[M+H]+1	229840977.3
19	Daidzin	$C_{21}H_{20}O_9$	416.10973	417.117	11.099	[M+H]+1	4461194759
20	Formononetin	$C_{16}H_{12}O_4$	268.07319	269.08041	15.656	[M+H]+1	916718307.7
21	5-Hydroxymethyl-2-furaldehyde	$C_6H_6O_3$	126.03185	127.03911	5.756	[M+H]+1	1585043775
22	Isoliquiritigenin	$C_{15}H_{12}O_4$	256.0732	257.08047	11.699	[M+H]+1	1469255594
23	Stearamide	$C_{18}H_{37}NO$	283.28683	284.2941	22.563	[M+H]+1	9711413331
24	Daidzein	$C_{15}H_{10}O_4$	254.05755	255.06482	13.918	[M+H]+1	1679347255
25	Isoliquiritigenin	$C_{15}H_{12}O_4$	256.07325	257.08051	13.455	[M+H]+1	199840368.8
26	Tangeritin	$C_{20}H_{20}O_7$	372.1203	373.12756	17.322	[M+H]+1	511627176.1
27	Quercetin-3β-D-glucoside	$C_{21}H_{20}O_{12}$	464.09538	465.10266	12.787	[M+H]+1	554677094.2
28	(2R,3R,4R,5R,6R)-2-({[(2S,3R,4R)-3,4-dihydroxy-4-(hydroxymethyl)oxolan-2-yl]oxy}methyl)-6-[2-(3,4-dimethoxyphenyl)ethoxy]-5-hydroxy-4-{[(2S,3R,4R,5R,6S)-3,4,5-trihydroxy-6-methyloxan-2-yl]oxy}oxan-3-yl (2E)-3-(3,4-dihydroxyphenyl)prop-2-enoate	$C_{36}H_{48}O_{19}$	801.30455	802.31183	12.797	[M+H]+1	640439047.6
29	Daidzein	$C_{15}H_{10}O_4$	254.05725	255.0645	11.102	[M+H]+1	445915100
30	Cryptotanshinone	$C_{19}H_{20}O_3$	296.14094	297.14822	18.527	[M+H]+1	760112826.2
31	DL-Homoserine	$C_4H_9NO_3$	119.05843	120.0657	1.25	[M+H]+1	620997867.1
32	Formononetin	$C_{16}H_{12}O_4$	268.07317	269.08032	13.214	[M+H]+1	160592585.8
33	D-(-)-Quinic acid	$C_7H_{12}O_6$	192.06343	193.07079	1.677	[M+H]+1	577148117.6

Table 3 High Resolution Mass Spectrometry Data and Elemental Composition of LCG (Negative Ion Mode)

No.	Name	Formula	MW	m/z	RT (min)	Ionization	Area
1	Daidzein	$C_{15}H_{10}O_4$	254.05743	253.05017	12.713	[M-H]-1	828737874.1
2	Formononetin	$C_{16}H_{12}O_4$	268.07336	267.06616	14.44	[M-H]-1	351460765.2
3	Palmitic acid	$C_{16}H_{32}O_2$	256.23994	255.23265	22.434	[M-H]-1	29248342.72
4	Chlorogenic acid	$C_{16}H_{18}O_9$	354.09431	353.08713	9.788	[M-H]-1	7882669029
5	4-Hydroxybenzaldehyde	$C_7H_6O_2$	122.03531	121.02804	9.455	[M-H]-1	134462906.3
6	4-Oxoproline	$C_5H_7NO_3$	129.04117	128.03387	2.608	[M-H]-1	3165580430
7	Oleic acid	$C_{18}H_{34}O_2$	282.25568	281.24841	22.687	[M-H]-1	15527138.95

(*Continued*)

Table 3 (Continued).

No.	Name	Formula	MW	m/z	RT (min)	Ionization	Area
8	Citraconic acid	$C_5H_6O_4$	130.02534	129.01807	5.552	[M-H]-1	115322875
9	2,3-Dihydro-1-benzofuran-2-carboxylic acid	$C_9H_8O_3$	164.04616	163.03886	11.254	[M-H]-1	207464236.8
10	Terephthalic acid	$C_8H_6O_4$	166.0253	165.01802	9.625	[M-H]-1	205180049.1
11	Citraconic acid	$C_5H_6O_4$	130.02531	129.01804	4.712	[M-H]-1	106585282.8
12	Caffeic acid	$C_9H_8O_4$	180.04121	179.03391	10.015	[M-H]-1	491901112.6
13	Linoleic acid	$C_{18}H_{32}O_2$	280.24014	279.23288	21.944	[M-H]-1	11134208.73

was created and the mICP/MAP and AUA/MAP ratios were computed (Figure 2D). Results indicated that the administration of medium and high doses of SMBJ led to a significant enhancement in erectile function in rats compared to the control group (Figure 2E and F). These findings suggest that SMBJ may be a promising therapeutic agent for reducing blood glucose levels and enhancing gonadal function.

In order to deeply understand the relevant pathological mechanism, further pathological analysis was carried out. Histological analysis indicated a significant decrease in smooth muscle content and smooth muscle-to-collagen ratio in the corpus cavernosum of the DMED group compared to the control group, implying the initiation of fibrosis in the corpus cavernosum. Nevertheless, administration of medium and high doses of SMBJ effectively restored the smooth muscle composition and reduced fibrosis. Immunohistochemical assays revealed that treatment with SMBJ resulted in a significant reduction in the expression of collagen I and collagen IV, while increasing the expression of SMA compared to the DMED group (Figure 3A–E). Furthermore, SMBJ treatment at medium and high doses effectively reversed the decrease in eNOS and nNOS levels in rat penile tissue associated with DMED (Figure 4A–C). ELISA analysis indicated a significant elevation in MDA expression and a marked decrease in cGMP, NO, and SOD levels in the penile tissue of rats in the DMED group compared to the control group (Figure 4D–G). Nevertheless, treatment with medium and high doses of SMBJ led to a notable decrease in MDA levels and an elevation in cGMP, NO, and SOD levels compared to the DMED group (Figure 4D–G). Transmission electron microscopy (TEM) analysis demonstrated significant damage to penile smooth muscle cells (SMCs) and vascular endothelial cells (VECs) in GK rats with DMED in comparison to the control group (Figures 3A and 4A). However, this damage was partially alleviated following treatment with medium and high doses of SMBJ.

Integrative Analysis of Network Pharmacology and Proteomics to Identify Key Targets of SMBJ for DMED

To explore the potential targets of SMBJ in DMED, the active components of the herbal medicines in SMBJ and their potential targets (human proteins) were identified using the HERB database (Table 4). Notably, 2229 drug targets predicted by network pharmacology were compared with 200 differentially expressed proteins detected by proteomics, among which 24 were identical, including AKT1, ASNS, and et al (Figure 5A). To identify targets specifically related to the DMED, we screened the target genes related to type 2 diabetes and ED annotated in the CTD database (association score>20) and selected the common annotated targets for both. Additionally, PPI network analysis identified the top 13 core erectile disorder-related target genes, based on the degree value and their interaction networks. Notably, AKT1 had the most connections with other protein genes encoded by the candidate genes (Figure 5B). Additionally, 235 key targets predicted by network pharmacology were compared with 489 drug molecules identified in SMBJ via mass spectrometry (according to the structural formula), among which 63 were identical. Among the molecules, three (C15H10O6, C15H10O7, C15H12O5) could bind to AKT1. Based on the mass spectrometry analysis results and the STRING database search, four active components of SMBJ (kaempferol, luteolin, naringenin, quercetin) were identified, all of which can interact with AKT1 (Figure 5C and Table 4). Furthermore, DMED-related regulatory pathways were identified via GO and KEGG pathway enrichment analysis of DMED-related genes. The top 10 enriched pathways included the P13K-Akt, calcium, extranuclear oestrogen, ERBB, ERS, FLT3, PTK6, hedgehog, MAPK, and VEGF signalling pathways (Figure 5D and E).

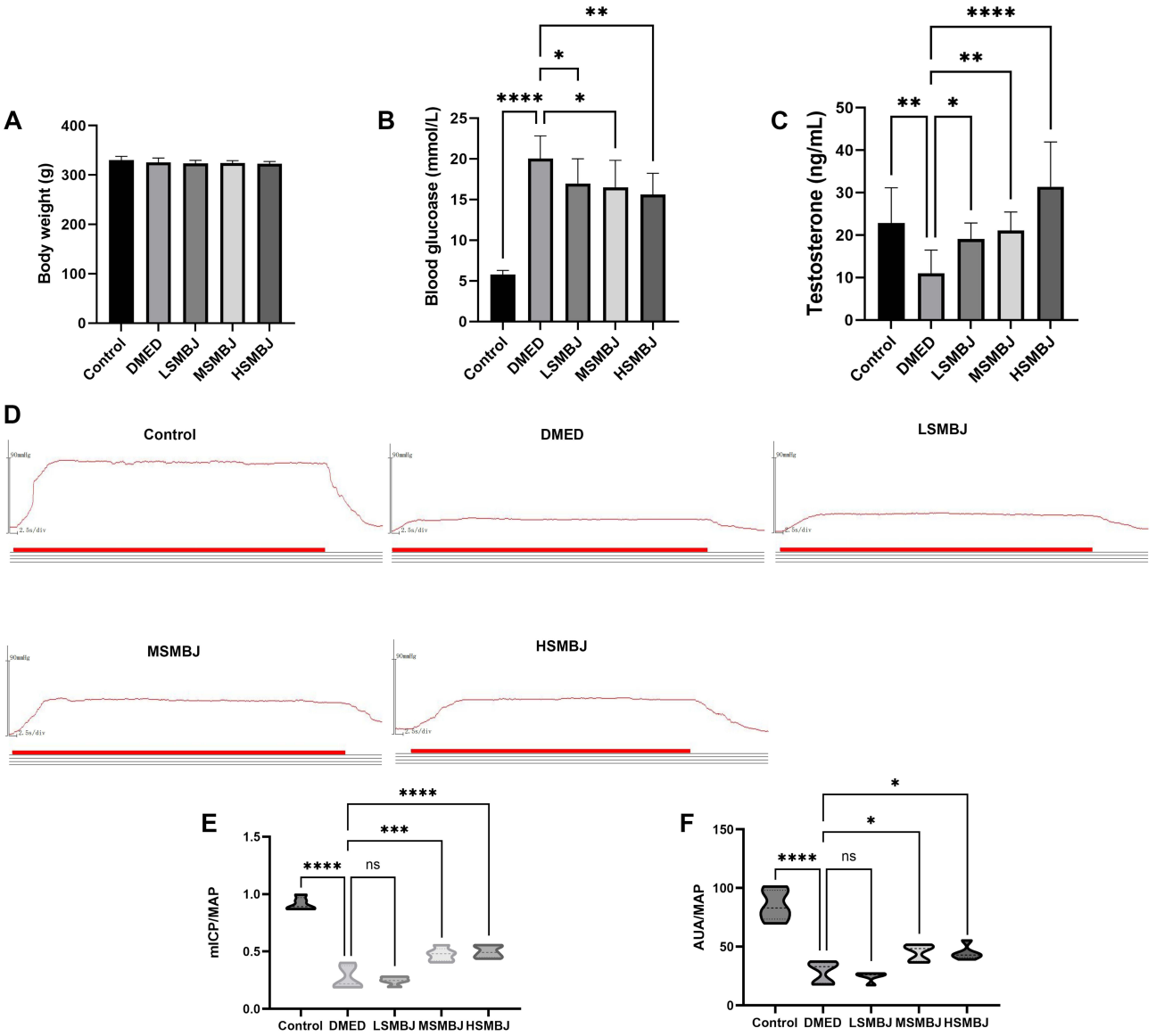

Figure 2 Assessment of treatment efficacy following SMBJ to GK rats. Body weight (**A**), blood glucose levels (**B**), and testosterone levels (**C**) of the rats with diabetes at the conclusion of the experiment (n = 10). (**D**) The ICP measurement surgery in GK rats after intragastric administration (n = 10). ICP representative images under electrical stimulation of the cavernous nerve. Bar graph of mICP/MAP (**E**) and AUA/MAP (**F**) ratios. Data shown are mean ± standard deviation. *P< 0.05, **P< 0.01, ***P< 0.001, ****P< 0.0001.

Effects of SMBJ on the Expression of the AKT Pathway in Rats With DMED

To elucidate the involvement of the PI3K/AKT signaling pathway in the therapeutic efficacy of SMBJ in DMED, we assessed the expression of key proteins related to this pathway, as well as those involved in vasodilation, angiogenesis, oxidative stress, and tissue stability, in penile tissue of DMED rats using Western blot analysis. Compared to the normal control group, the phosphorylated AKT1 to total AKT1 (p-AKT1/AKT1) protein ratio was significantly elevated in the DMED group (P<0.05), indicating activation of the PI3K/AKT signaling pathway under diabetic conditions. However, SMBJ treatment further significantly increased the levels of PI3K, p-AKT1/AKT1, and neuronal nitric oxide synthase (nNOS) proteins, while markedly reducing the nuclear factor-kappa B (NF-κB) protein level in penile tissue compared to the DMED group (P<0.05) (Figure 6A–D).

Interestingly, SMBJ treatment also reversed changes in the expression of certain regulatory proteins linked to DMED pathophysiology. Protein tyrosine phosphatase non-receptor type 12 (PTPN12) is a tyrosine phosphatase that modulates multiple signaling pathways, including the MAPK/ERK and PI3K/AKT cascades, by dephosphorylation, thereby

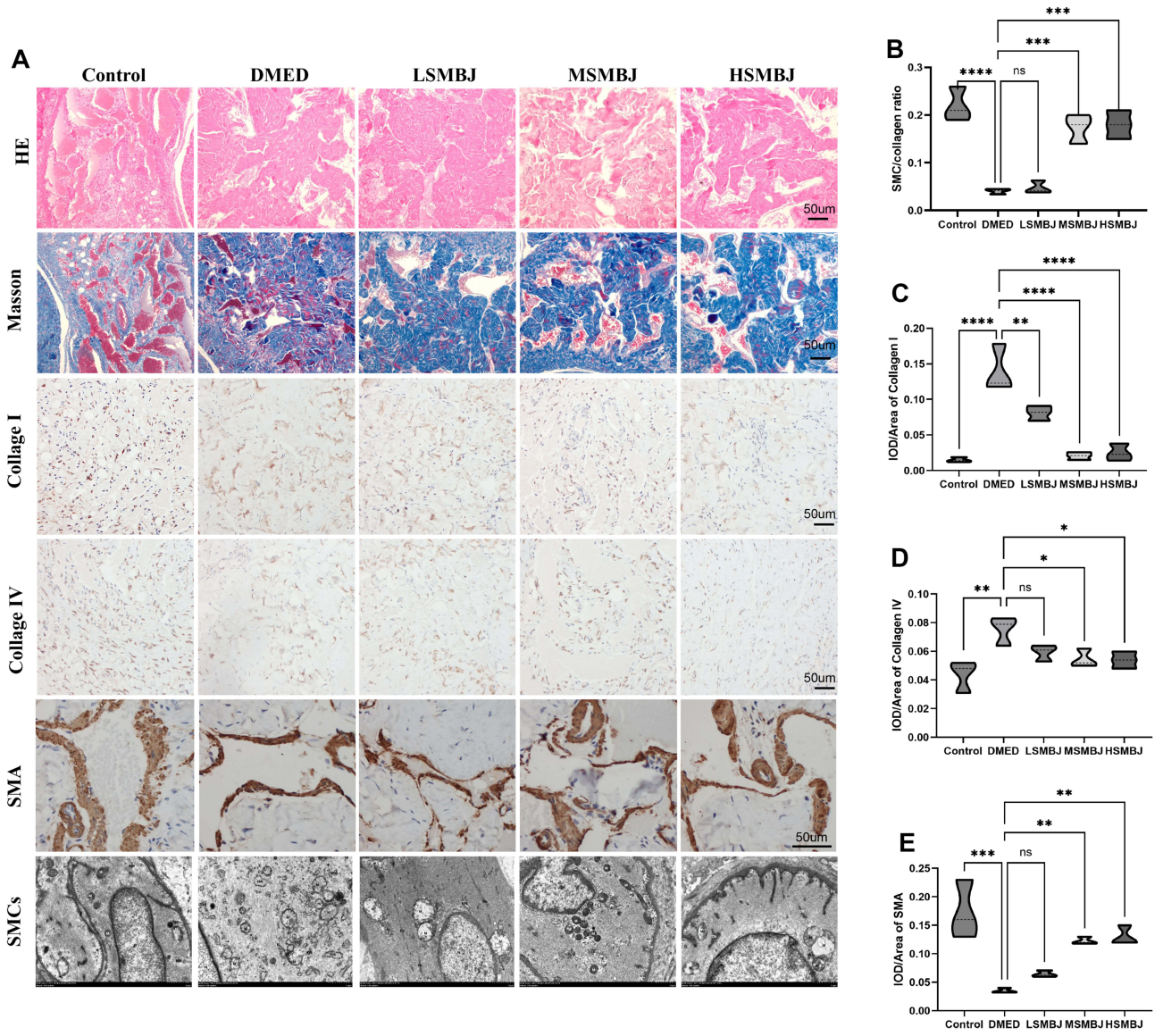

Figure 3 Evaluation of the therapeutic effect of SMBJ on penile fibrosis in GK rats. (**A**) H&E, Masson's trichrome and Immunohistochemistry (IHC) of Collage I, Collage IV and SMA staining in a penile midshaft specimen (n = 5). The penile smooth muscle cells (SMCs) of GK rats were observed by TEM. Bar graph of SMC/collagen (**B**), CollagenI (**C**), Collagen IV (**D**) and SMA (**E**) ratios. Data shown are mean ± standard deviation. *P< 0.05, **P< 0.01, ***P< 0.001, ****P< 0.0001.

influencing the survival and functionality of endothelial cells and neurons.[27] Asparagine synthetase (ASNs) are crucial enzymes that catalyze the synthesis of asparagine from aspartate and glutamine, playing a pivotal role in cellular metabolism and stress responses.[28] Specifically, the protein levels of PTPN12 were significantly elevated in the SMBJ-treated group, suggesting a restoration of its regulatory role in vascular homeostasis. In contrast, CBPA1 protein levels were markedly reduced, further aligning with the improvement in vascular and metabolic stability (P<0.05). However, the expression of ASNs, a protein implicated in cellular stress responses and metabolic adaptation, showed no significant changes (P>0.05) (Figure 6A–D).

These findings emphasize the pivotal role of the PI3K/AKT signaling pathway in modulating oxidative stress, endothelial function, and angiogenesis in DMED. The significant reduction in NF-κB levels suggests a dampening of pro-inflammatory responses, while the increased expression of PTPN12 further highlights its potential involvement in maintaining endothelial stability and mitigating vascular abnormalities in DMED. Collectively, these results support the mechanistic involvement of PI3K/AKT signaling and associated proteins in the therapeutic benefits of SMBJ for DMED.

https://doi.org/10.2147/DDDT.S495366

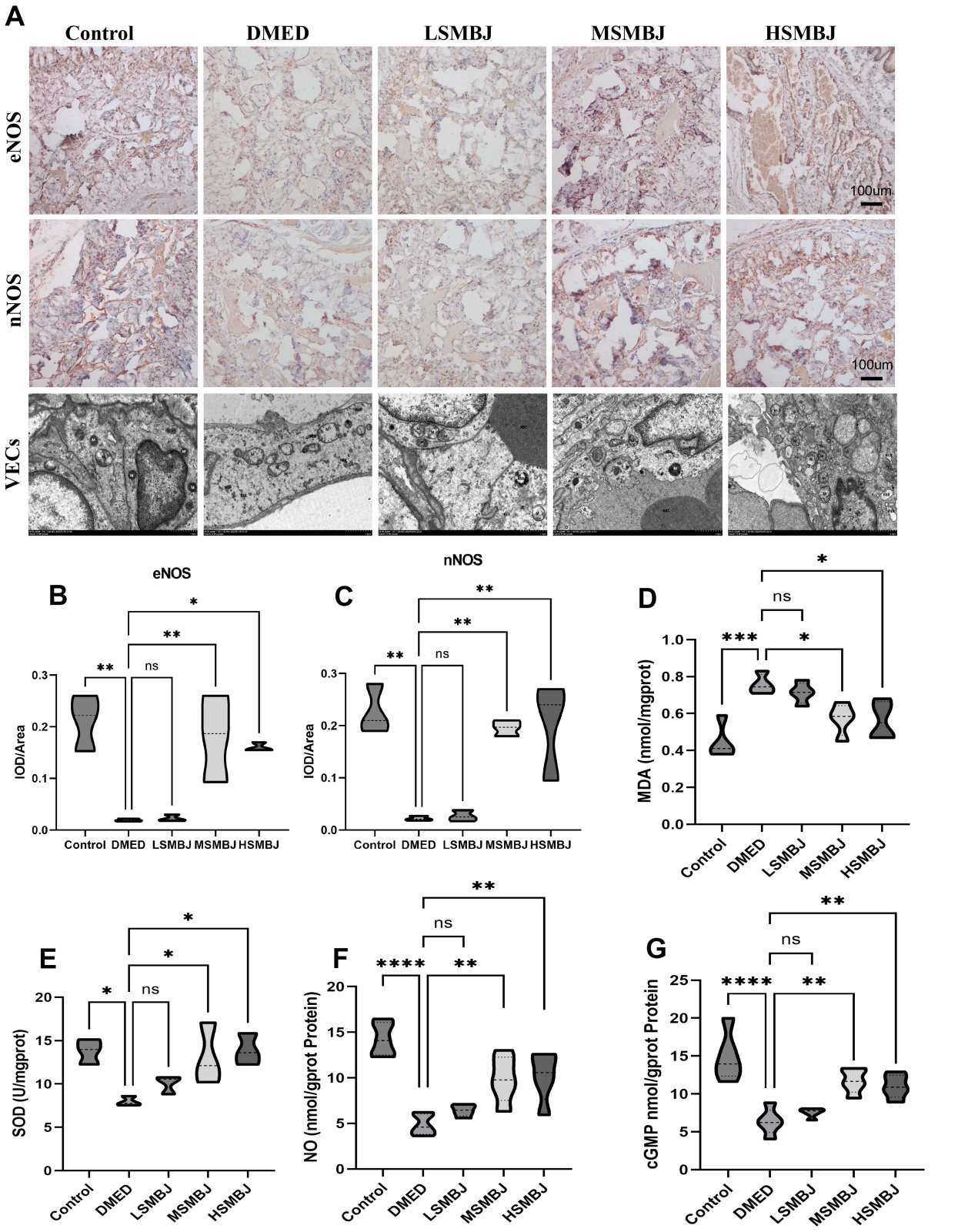

Figure 4 Evaluation of therapeutic effect of SMBJ on penile vascular function in GK rats. (**A**) Immunohistochemistry (IHC) of eNOS, nNOS and TEM of VECs (n = 5). Bar graph of eNOS (**B**), nNOS (**C**). ELISA assay for the penile tissue of MDA (**D**), SOD (**E**), NO (**F**) and cGMP (**G**) levels. Data shown are mean ± standard deviation. **P*< 0.05, ***P*< 0.01, ****P*< 0.001, *****P*< 0.0001.

 https://doi.org/10.2147/DDDT.S495366

Table 4 Durg Compounds Analysis of SMBJ

Herb Pinyin Name	Herb ID	Scientific Name	Herb Latin Name	Ingredient name	Ingredient_formula	PubChem_ID
DANSHEN	HERB001193	Salvia miltiorrhiza Bunge	RadixSalviaeliguliobae	Kaempferol	$C_{15}H_{10}O_6$	5280863
GANCAO	HERB001779	Glycyrrhiza uralensis Fisch	RadixGlycyrrhizae	Kaempferol	$C_{15}H_{10}O_6$	5280863
HUANGQI	HERB002560	Astragalus membranaceus var. membranaceus	RadixAstragali	Kaempferol	$C_{15}H_{10}O_6$	5280863
JINYINHUA	HERB002962	Lonicera japonica	FlosLonicerae	Kaempferol	$C_{15}H_{10}O_6$	5280863
YINYANGHUO	HERB006633	Epimedium brevicornu	EpimrdiiHerba	Kaempferol	$C_{15}H_{10}O_6$	5280863
DANSHEN	HERB001193	Salvia miltiorrhiza Bunge	RadixSalviaeliguliobae	Luteolin	$C_{15}H_{10}O_6$	5280445
JINYINHUA	HERB002962	Lonicera japonica	FlosLonicerae	Luteolin	$C_{15}H_{10}O_6$	5280445
YINYANGHUO	HERB006633	Epimedium brevicornu	EpimrdiiHerba	Luteolin	$C_{15}H_{10}O_6$	5280445
GANCAO	HERB001779	Glycyrrhiza uralensis Fisch	RadixGlycyrrhizae	Naringenin	$C_{15}H_{12}O_5$	667495
DANSHEN	HERB001193	Salvia miltiorrhiza Bunge	RadixSalviaeliguliobae	Quercetin	$C_{15}H_{10}O_7$	5280343
GANCAO	HERB001779	Glycyrrhiza uralensis Fisch	RadixGlycyrrhizae	Quercetin	$C_{15}H_{10}O_7$	5280343
GOUQIZI	HERB001915	Lycium chinense	FructusLycii	Quercetin	$C_{15}H_{10}O_7$	5280343
HUANGLIAN	HERB002540	Coptis chinensis	RhizomaCoptidis	Quercetin	$C_{15}H_{10}O_7$	5280343
HUANGQI	HERB002560	Astragalus membranaceus var. membranaceus	RadixAstragali	Quercetin	$C_{15}H_{10}O_7$	5280343
JINYINHUA	HERB002962	Lonicera japonica	FlosLonicerae	Quercetin	$C_{15}H_{10}O_7$	5280343
LIZHIHE	HERB003348	Litchi chinensis	SemenLitchi	Quercetin	$C_{15}H_{10}O_7$	5280343
YINYANGHUO	HERB006633	Epimedium brevicornu	EpimrdiiHerba	Quercetin	$C_{15}H_{10}O_7$	5280343

Consistent Drug-Binding Pockets Between Humans and Rats on ATK1

Drug-binding pockets in humans and rats were predicted using the CurPocket method in CB-Dock. The sequence-level similarity of the primary structure reached 98%, and the water similarity of the three-dimensional structure reached 0.9 (value range: 0–1) (Figure 7A). Notably, the amino acid molecules bound to the pocket were identical to the 3D structural diagrams of proteins in humans and rats (Figure 7B and C). Finally, Figure 7D illustrates that these consistent molecular features across species suggest that SMBJ likely shares a common molecular mechanism of action in both humans and rats. Overall, the predicted drug-binding pockets indicate that SMBJ has a common molecular mechanism of action in humans and rats.

Key Substrate Protein AKT1 Binding to Core Molecule Luteolin

The high-throughput virtual molecule screening software InstaDock was used for automated blind docking to assess the binding potential of the active ingredients to the predicted target (AKT1). Among the active compounds in SMBJ, luteolin showed the highest binding activity for human-rat AKT1 (Figure 8A). Additionally, three other drug molecules (kaempferol, quercetin, naringenin) showed good binding affinity for AKT1 (Figure 8D–F). Moreover, mass spectrometry confirmed the presence of luteolin in SMBJ (Figure 8B). To probe the direct relationship between the core targets and corresponding active components in SMBJ and the binding mode of the core target compound, we performed molecular docking. Two types of reciprocities were detected using the protein-ligand interaction profiler tool, namely hydrogen and hydrophobic bonds (Figure 8C).

Discussion

Endothelial dysfunction of microvascular origin and the delayed restoration may contribute to diabetic microvascular complications.[29] In order to address the limited effectiveness of initial anti-PED5 medications (44%) and the intricate development of DMED, it is essential for patients with treatment resistant DMED to undergo combination therapy

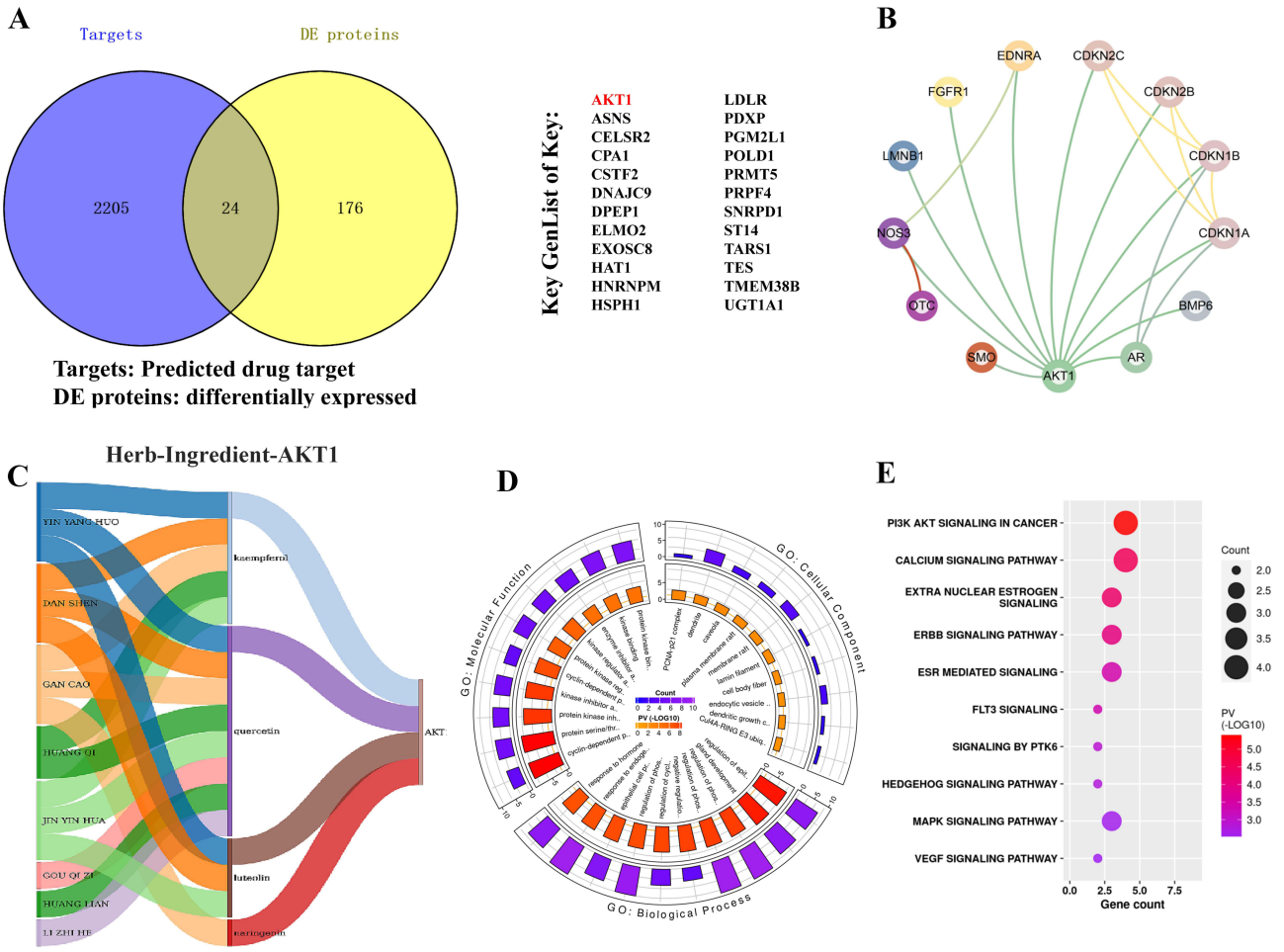

Figure 5 Integrating analyses of omics and network pharmacology. (**A**) Comparison of key network pharmacological targets and differential proteins. (**B**) Erectile disorder related genes and their interaction networks. (**C**) Relationship between SMBJ herbal ingredients and AKT1, a key gene in erectile dysfunction in DMED. (**D**) GO enrichment analysis of Erectile disorder related gene regulatory pathways. (**E**) KEGG enrichment analysis of Erectile disorder related gene regulatory pathways.

targeting multiple factors. This study explored the therapeutic benefits and molecular mechanisms of SMBJ in the treatment of DMED through the utilisation of proteomic techniques, molecular docking, and network pharmacology.

SMBJ is composed of 13 TCMs with complex components and diverse functions. For example, *Carapax trionycis, Radix salviae liguliobae, Radix scrophulariae, Semen litchi, Radix astragali*, and *Radix angelicae* have a potent antifibrotic effect.[30–34] Additionally, *Radix puerariae, Radix salviae*, and *Radix rehmanniae preparata* contribute to vasodilation and angiogenesis,[35–37] while *Radix salviae liguliobae, Fructus lycii, Epimrdii herba*, honeysuckle, and *Rhizoma coptidis* exhibit significant antioxidative properties.[31,38–40] *Radix glycyrrhizae* plays a role in reducing toxicity at the cellular level.[41] In the present study, we thoroughly examined the constituents present in the SMBJ acetone extract. Out of the identified active substances, 64 were utilised in DMED therapy. To investigate the therapeutic effects of SMBJ on DMED, we examined the impact of different doses of SMBJ on erectile function using a non-obese type 2 diabetic animal model, the GK rat. The results showed that SMBJ significantly improved erectile function and ameliorated DMED by reducing corpus cavernosum fibrosis, decreasing eNOS and nNOS levels, alleviating oxidative stress in penile tissue, and mitigating damage to SMCs and VECs. This suggests that SMBJ could be a potential traditional Chinese medicine for treating DMED. The core drug component, luteolin, is a naturally occurring tetrahydroxy flavone[42] found in several edible plants, including *Radix salviae liguliobae, Flos lonicerae*, and *Epimrdii herba*. Research evidence suggests that luteolin exerts protective effects on the cardiovascular system. For example, luteolin relaxes thoracic aortic rings and uterine arterial blood vessels in rats in an endothelium-dependent manner mainly by stimulating the NOS pathway.[43,44] Additionally, luteolin protects against hypertension and vascular complications associated with diabetes by improving NO generation to promote vasodilation.[44,45] Moreover, luteolin exerts anti-inflammatory and antioxidant effects

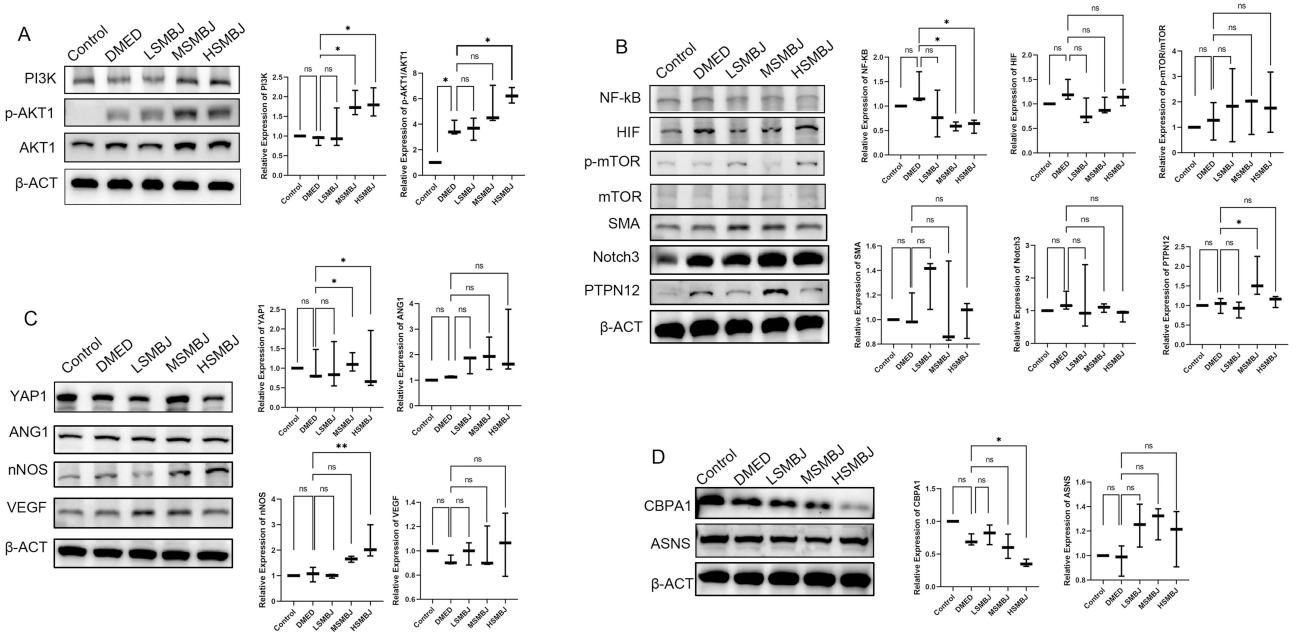

Figure 6 The pathway enrichment proteins analysis of SMBJ in the penile tissues. The penile tissues of five group Western blot results of PI3K and p-AKT1/AKT1 (**A**), NF-kB, HIF, p-mTOR/mTOR, SMA, Notch3 and PTPN12 (**B**), YAP1, ANG1, nNOS and VEGF (**C**), CBPA1 and ASNS (**D**) (n = 5). Data shown are mean ± standard deviation. **P*< 0.05, ***P*< 0.01.

through the PI3K/AKT pathway.[46,47] Based on these findings, luteolin as a core drug component of SMBJ represents the treatment potential for DMED treatment. Luteolin is one of the core drug components of SMBJ. Additionally, through network pharmacology and proteomics analysis of rat penile tissue, we identified AKT1 as a therapeutic target of SMBJ in DMED.

AKT1, also known as the phosphoinositide 3-kinase (PI3K)-AKT signalling pathway, regulates protein biosynthesis, growth and survival of cells, and neovascularisation.[48–52] Notably, angiogenesis can be promoted, and vascular stability can be improved via PI3K/Akt signalling pathway stimulation-induced expression of ASNS, VEGF, and Ang1.[49,51,53–55] Additionally, upregulation of the PI3K/AKT/nNOS pathway can increase NO production.[56,57] Therefore, enhancing the PI3K/Akt to contribute to the expression of nNOS, NO is a potential strategy for improving erectile function in rats with DMED.[8] Therefore, it can be concluded that SMBJ may prevent DMED development by targeting AKT1. To validate this hypothesis, we employed Western blotting and molecular docking to elucidate the mechanisms of action of the key active compound, luteolin, on the core drug target AKT1. The results demonstrated that luteolin in SMBJ regulates the PI3K/Akt/nNOS and NF-kB signaling pathways, enhances vascular dilation and contraction, and reduces oxidative stress levels, thereby improving erectile dysfunction in DMED rats. Molecular docking results also indicated that luteolin exhibited the highest binding activity to both human and rat AKT1. Interestingly, the amino acid molecules binding to the pocket were consistent with the 3D structural maps of human and rat proteins. The predicted drug-binding pockets suggest a shared molecular mechanism of SMBJ action in humans and rats. Therefore, although clinical validation is yet to be performed, the findings suggest that SMBJ may have a beneficial therapeutic effect on erectile dysfunction in clinical DMED patients. Overall, these findings revealed the active drug compounds in SMBJ and potential therapeutic targets in DMED, offering a theoretical foundation for utilising SMBJ in the treatment of DMED.

Despite the promising results in the present study, we solely validated the identified objectives via computer simulations and GK rat model experiments without conducting in vivo experiments. The effects of SMBJ were not compared with other hypoglycaemic and anti-PED5 drugs, and a combined intervention was not conducted for further assessment. Therefore, additional studies are necessary to compare the mechanisms and therapeutic effects of SMBJ and other hypoglycaemic and anti-PED5 drugs in vivo, as well as well-designed cell experiments in vitro.

This study has several limitations that should be considered when interpreting the results. First, the inherent individual variability of the DMED rat model may influence experimental outcomes despite efforts to minimize confounding factors through strict inclusion criteria, randomization, and increased replication. Variations in metabolic

A

Entry	Chain	RMSD	TM-score	Identity	Equivalent Residues	Sequence Length
human	A	-	-	-	-	480
rat	A	2.77	0.9	98%	480	480

B

Spatial level (three-dimensional structure) similarity

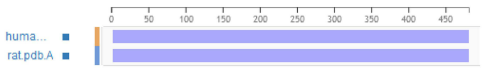

C

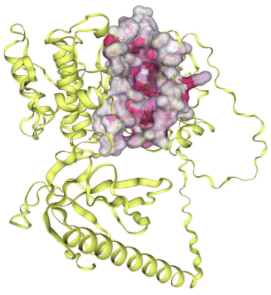

Human-AKT1

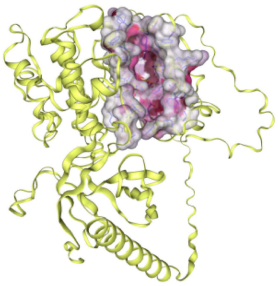

Rat-AKT1

Species	Cavity volume (Å^3)	Center (x, y, z)	Cavity size (x, y, z)
Human	1912	-3, -7, 8	15, 29, 15
Rat	1881	-3, -4, 10	15, 26, 13

D

Human AKT1 protein binding pocket composition amino acids

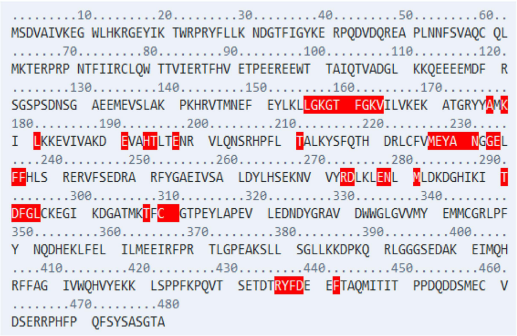

Rat AKT1 protein binding pocket composition amino acids

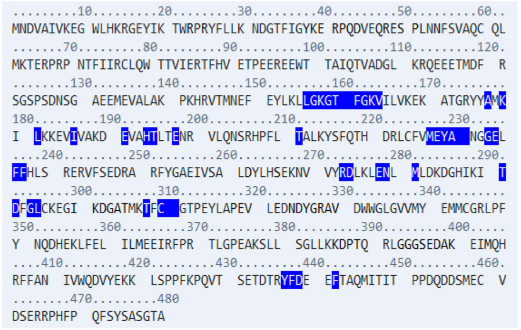

Figure 7 Display of core molecule luteolin results. (**A**) Summary Table for Comparison of Sequence Composition and 3D Structural Similarity. (**B**) 3D structural similarity comparison diagram. (**C**) Using the CurPocket method of the CB Dock toolkit to predict drug binding pockets that are consistent between humans and rats. (**D**)The amino acid molecules bound to the pocket are also basically the same.

state, endothelial dysfunction progression, and response to hyperglycemia could subtly affect the observed therapeutic efficacy of SMBJ. Second, the sample size, while sufficient for preliminary analysis, may not fully capture broader population variability, and the lack of multi-center validation limits the generalizability of the findings. Furthermore, certain metabolic and physiological variables may not have been entirely controlled. Additionally, the absence of in vitro experiments represents another limitation, as it restricts our ability to fully elucidate the molecular and signaling mechanisms underlying SMBJ's effects. While this study primarily relied on in vivo models and network pharmacology approaches, further validation at the cellular level is needed. In particular, the PI3K/Akt signaling pathway and its downstream targets, which were highlighted in our findings, warrant further investigation through in vitro studies, such as

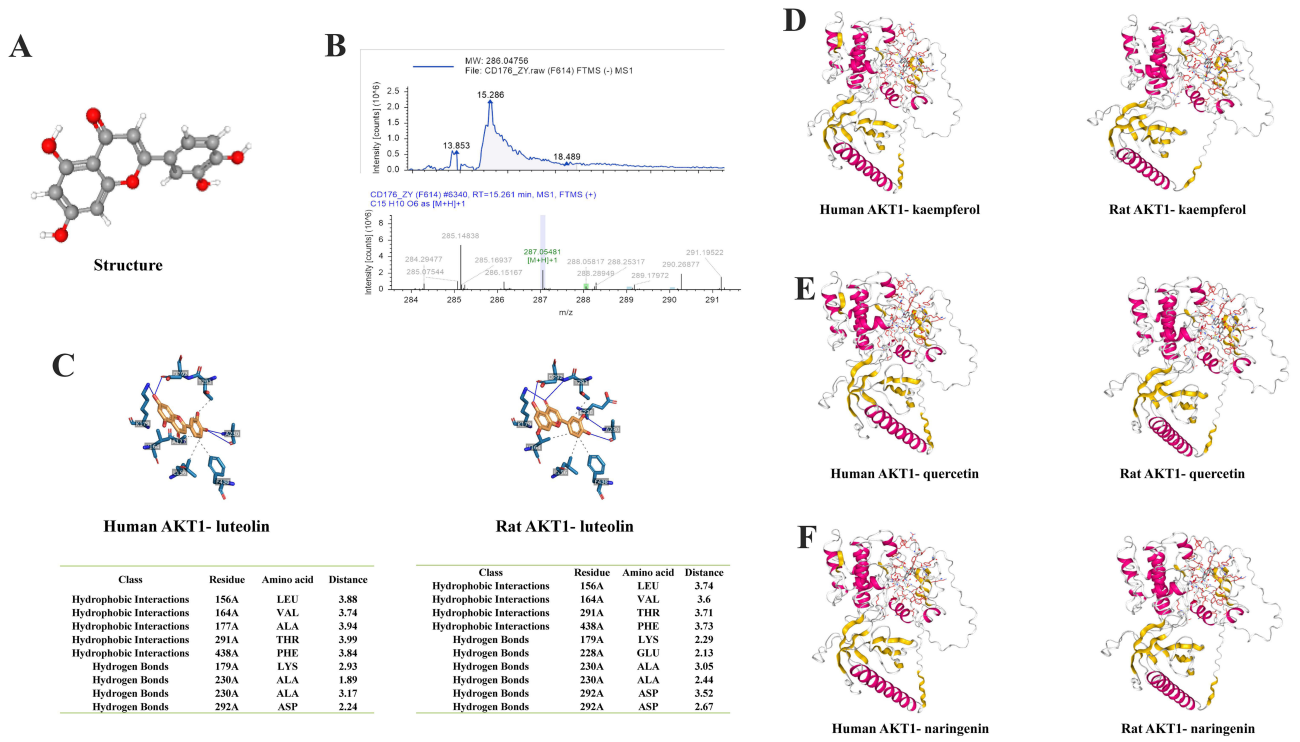

Class	Residue	Amino acid	Distance
Hydrophobic Interactions	156A	LEU	3.88
Hydrophobic Interactions	164A	VAL	3.74
Hydrophobic Interactions	177A	ALA	3.94
Hydrophobic Interactions	291A	THR	3.99
Hydrophobic Interactions	438A	PHE	3.84
Hydrogen Bonds	179A	LYS	2.93
Hydrogen Bonds	230A	ALA	1.89
Hydrogen Bonds	230A	ALA	3.17
Hydrogen Bonds	292A	ASP	2.24

Class	Residue	Amino acid	Distance
Hydrophobic Interactions	156A	LEU	3.74
Hydrophobic Interactions	164A	VAL	3.6
Hydrophobic Interactions	291A	THR	3.71
Hydrophobic Interactions	438A	PHE	3.73
Hydrogen Bonds	179A	LYS	2.29
Hydrogen Bonds	228A	GLU	2.13
Hydrogen Bonds	230A	ALA	3.05
Hydrogen Bonds	230A	ALA	2.44
Hydrogen Bonds	292A	ASP	3.52
Hydrogen Bonds	292A	ASP	2.67

Figure 8 Human and rat AKT1-luteolin protein-drug interaction. (**A**) Molecular structure of luteolin. (**B**) Check the spectrum of the detected drug molecule luteolin in the mass spectrometry. (**C**) Human and rat AKT1-luteolin protein-drug interaction prediction by molecular docking. (**D**) Human and rat AKT1-kaempferol protein-drug interaction prediction. (**E**) Human and rat AKT1-quercetin protein-drug interaction prediction. (**F**) Human and rat AKT1-naringenin protein-drug interaction prediction.

endothelial or smooth muscle cell models under diabetic conditions, to dissect direct protein interactions and functional roles. The study did not compare these extracted substances with standard drugs to determine if they are equivalent. To address these limitations, future research should incorporate larger, more diverse sample sizes, conduct multi-center studies, and employ advanced molecular techniques, such as single-cell RNA sequencing and protein interaction analyses. Moreover, in vitro experiments, including pathway-specific interventions, will be essential to validate and refine our current findings, further strengthening the mechanistic understanding of SMBJ in DMED treatment.

Conclusion

Network pharmacology, proteomics, and animal experiments indicated that SMBJ ameliorated DMED in rats via PI3K/Akt/nNOS and NF-kB signaling pathways to increase the levels of eNOS and nNOS, reduce oxidative stress levels and improve the angiogenesis and stability in penile tissue. Notably, molecular docking showed that the therapeutic effects of SMBJ were attributable to its luteolin content, as luteolin had the strongest binding activity for AKT1 in the penile tissue of rats with DMED. Overall, this study revealed the potential therapeutic targets of SMBJ in DMED, providing a theoretical basis for SMBJ application in DMED treatment.

Abbreviations

TEM, transmission electron microscopy; ICP, intracavernous pressure; MAP, mean arterial blood pressure; AUA, area under the curve; Ang-1, Angiopoietin-1; SMBJ, Simiao Biejia; DMED, diabetes mellitus-induced erectile dysfunction; MDA, malondialdehyde; SOD, superoxide dismutase; VEGF, vascular endothelial growth factor; VECs, vascular endothelial cells; SMCs, smooth muscle cells; ED, erectile dysfunction; GO, Gene Ontology; KEGG, Kyoto Encyclopedia of Genes and Genomes; GK, Goto-Kakisaki.

Data Sharing Statement

All datasets generated and analyzed in this current study are available in the manuscript.

https://doi.org/10.2147/DDDT.S495366

Acknowledgments

The researchers and staff of the software and databases are greatly appreciated by the authors. We are thankful for the support of the data analysts. We would like to thank Editage (www.editage.cn) for English language editing.

Author Contributions

All authors contributed to data analysis, drafting or revising the article, have agreed on the journal to which the article will be submitted, gave final approval of the version to be published, and agree to be accountable for all aspects of the work.

Funding

This research was supported by the Joint Funds of the National Natural Science Foundation of China (82074440 to BJ, 82374459 to DS and 82171593 to YC).

Disclosure

The authors report no conflicts of interest in this work.

References

1. Ayta IA, McKinlay JB, Krane RJ. The likely worldwide increase in erectile dysfunction between 1995 and 2025 and some possible policy consequences. *BJU Int*. 1999;84(1):50–56. doi:10.1046/j.1464-410x.1999.00142.x
2. Shiferaw WS, Akalu TY, Petrucka PM, Areri HA, Aynalem YA. Risk factors of erectile dysfunction among diabetes patients in Africa: a systematic review and meta-analysis. *J Clin Transl Endocrinol*. 2020;21:100232. doi:10.1016/j.jcte.2020.100232
3. Gatti A, Mandosi E, Fallarino M, et al. Metabolic syndrome and erectile dysfunction among obese non-diabetic subjects. *J Endocrinol Invest*. 2009;32(6):542–545. doi:10.1007/bf03346504
4. Barkabi-Zanjani S, Ghorbanzadeh V, Aslani M, Ghalibafsabbaghi A, Chodari L. Diabetes mellitus and the impairment of male reproductive function: possible signaling pathways. *Diabetes Metab Syndr*. 2020;14(5):1307–1314. doi:10.1016/j.dsx.2020.07.031
5. Newsholme P, Haber EP, Hirabara SM, et al. Diabetes associated cell stress and dysfunction: role of mitochondrial and non-mitochondrial ROS production and activity. *J Physiol*. 2007;583(Pt 1):9–24. doi:10.1113/jphysiol.2007.135871
6. Kma L, Baruah TJ. The interplay of ROS and the PI3K/Akt pathway in autophagy regulation. *Biotechnol Appl Biochem*. 2022;69(1):248–264. doi:10.1002/bab.2104
7. Bhatt MP, Lee YJ, Jung SH, et al. C-peptide protects against hyperglycemic memory and vascular endothelial cell apoptosis. *J Endocrinol*. 2016;231(1):97–108. doi:10.1530/joe-16-0349
8. Ma JX, Wang B, Li HS, et al. Uncovering the mechanisms of leech and centipede granules in the treatment of diabetes mellitus-induced erectile dysfunction utilising network pharmacology. *J Ethnopharmacol*. 2021;265:113358. doi:10.1016/j.jep.2020.113358
9. Maxwell AJ. Mechanisms of dysfunction of the nitric oxide pathway in vascular diseases. *Nitric Oxide*. 2002;6(2):101–124. doi:10.1006/niox.2001.0394
10. Chen CY, Chang YH, Bau DT, et al. Discovery of potent inhibitors for phosphodiesterase 5 by virtual screening and pharmacophore analysis. *Acta Pharmacol Sin*. 2009;30(8):1186–1194. doi:10.1038/aps.2009.100
11. Liu DF, Jiang H, Hong K, Zhao LM, Tang WH, Ma LL. Influence of erectile dysfunction course on its progress and efficacy of treatment with phosphodiesterase type 5 inhibitors. *Chin Med J*. 2010;123(22):3258–3261. doi:10.3760/cma.j.issn.0366-6999.2010.22.016
12. Cai Z, Song X, Zhang J, Yang B, Li H. Practical Approaches to Treat ED in PDE5i Nonresponders. *Aging Dis*. 2020;11(5):1202–1218. doi:10.14336/ad.2019.1028
13. Seto SW, Chang D, Kiat H, Wang N, Bensoussan A. Chinese herbal medicine as a potential treatment of abdominal aortic aneurysm. *Front Cardiovasc Med*. 2018;5:33. doi:10.3389/fcvm.2018.00033
14. Ding Y, Peng L, Lu SC. [Current research situation of atherosclerotic vulnerable plaque and discussion of the efficacy of simiao yongan decoction]. *Zhongguo Zhong xi yi jie he za zhi*. 2012;32(9):1287–1289. Danish
15. Huang J, Xu FS. [Erdi Biejia decoction for erectile dysfunction with kidney-yin deficiency]. *Zhonghua nan ke xue*. 2012;18(12):1143–1146. Basque
16. Crimmel AS, Conner CS, Monga M. Withered Yang: a review of traditional Chinese medical treatment of male infertility and erectile dysfunction. *J Andrology*. 2001;22(2):173–182. doi:10.1002/j.1939-4640.2001.tb02168.x
17. Luo B, Li Y, Wang W, et al. Clinical evidence and mechanisms of traditional Chinese medicine in major diseases. *Sci Tradit Chin Med*. 2023;1(1):3–13. doi:10.1097/st9.0000000000000009
18. Pang K, Pan D, Xu H, et al. Advances in physical diagnosis and treatment of male erectile dysfunction. *Front Physiol*. 2022;13:1096741. doi:10.3389/fphys.2022.1096741
19. Qiu X, Fandel TM, Ferretti L, et al. Both immediate and delayed intracavernous injection of autologous adipose-derived stromal vascular fraction enhances recovery of erectile function in a rat model of cavernous nerve injury. *Europ urol*. 2012;62(4):720–727. doi:10.1016/j.eururo.2012.02.003
20. Fang S, Dong L, Liu L, et al. HERB: a high-throughput experiment- and reference-guided database of traditional Chinese medicine. *Nucleic Acids Res*. 2021;49(D1):D1197–D1206. doi:10.1093/nar/gkaa1063
21. Davis AP, Grondin CJ, Johnson RJ, et al. Comparative Toxicogenomics Database (CTD): update 2021. *Nucleic Acids Res*. 2021;49(D1):D1138–D1143. doi:10.1093/nar/gkaa891

22. NCBI Resource Coordinators. Database resources of the National Center for Biotechnology Information. *Nucleic Acids Res*. 2014;42(Database issue):D7–D17. doi:10.1093/nar/gkt1146
23. Chen J, Bardes EE, Aronow BJ, Jegga AG. ToppGene Suite for gene list enrichment analysis and candidate gene prioritization. *Nucleic Acids Res*. 2009;37(Web Server issue):W305–W311. doi:10.1093/nar/gkp427
24. Liu Y, Grimm M, Dai WT, Hou MC, Xiao ZX, Cao Y. CB-Dock: a web server for cavity detection-guided protein-ligand blind docking. *Acta Pharmacol Sin*. 2020;41(1):138–144. doi:10.1038/s41401-019-0228-6
25. Jaganathan R, Kumaradhas P. Binding mechanism of anacardic acid, carnosol and garcinol with PCAF: a comprehensive study using molecular docking and molecular dynamics simulations and binding free energy analysis. *J Cell Biochem*. 2023;124(5):731–742. doi:10.1002/jcb.30400
26. Salentin S, Schreiber S, Haupt VJ, Adasme MF, Schroeder M. PLIP: fully automated protein-ligand interaction profiler. *Nucleic Acids Res*. 2015;43 (W1):W443–W447. doi:10.1093/nar/gkv315
27. Sivaganesh V, Sivaganesh V, Scanlon C, et al. Protein Tyrosine Phosphatases: mechanisms in Cancer. *Int J Mol Sci*. 2021;22(23):12865. doi:10.3390/ijms222312865
28. Wang X, Gong W, Xiong X, Jia X, Xu J. Asparagine: a key metabolic junction in targeted tumor therapy. *Pharmacol Res*. 2024;206:107292. doi:10.1016/j.phrs.2024.107292
29. Strain WD, Paldánius PM. Diabetes, cardiovascular disease and the microcirculation. *Cardiovasc Diabetol*. 2018;17(1):57. doi:10.1186/s12933-018-0703-2
30. Hu Z, You P, Xiong S, et al. Carapax Trionycis extracts inhibit fibrogenesis of activated hepatic stellate cells via TGF-β1/Smad and NFκB signaling. *Biomed Pharmacother*. 2017;95:11–17. doi:10.1016/j.biopha.2017.08.011
31. Jia Q, Zhu R, Tian Y, et al. Salvia miltiorrhiza in diabetes: a review of its pharmacology, phytochemistry, and safety. *Phytomedicine*. 2019;58:152871. doi:10.1016/j.phymed.2019.152871
32. Zhang Y, Gu L, Xia Q, Tian L, Qi J, Cao M. Radix astragali and radix angelicae sinensis in the treatment of idiopathic pulmonary fibrosis: a systematic review and meta-analysis. *Front Pharmacol*. 2020;11:415. doi:10.3389/fphar.2020.00415
33. Yan J, Feng Y, Fang X, et al. Anti-liver fibrosis effects of the total flavonoids of litchi semen on CCl(4)-induced liver fibrosis in rats associated with the upregulation of retinol metabolism. *Pharm Biol*. 2022;60(1):1264–1277. doi:10.1080/13880209.2022.2086584
34. Huang XY, Chen CX, Zhang XM, Liu Y, Wu XM, Li YM. Effects of ethanolic extract from Radix Scrophulariae on ventricular remodeling in rats. *Phytomedicine*. 2012;19(3–4):193–205. doi:10.1016/j.phymed.2011.09.079
35. Koon CM, Wing-Shing Cheung D, Wong PH, et al. Salviae miltiorrhizae radix and puerariae lobatae radix herbal formula improves circulation, vascularization and gait function in a peripheral arterial disease rat model. *J Ethnopharmacol*. 2021;264:113235. doi:10.1016/j.jep.2020.113235
36. Zhu HF, Wan D, Chen Y, Xu XY, Chen L, He ZG. [Effects of Rehmannia root decoction serum on cell proliferation and EPO expression in cultured human umbilical vein endothelial cells]. *Zhongguo Zhong yao za zhi*. 2008;33(13):1579–1582. Catalan
37. Yang Y, Wang Y, Deng Y, et al. Fructus Lycii and Salvia miltiorrhiza Bunge extract attenuate oxidative stress-induced photoreceptor ferroptosis in retinitis pigmentosa. *Biomed Pharmacother*. 2023;167:115547. doi:10.1016/j.biopha.2023.115547
38. Ran Q, Wang J, Wang L, Zeng HR, Yang XB, Huang QW. Rhizoma coptidis as a potential treatment agent for type 2 diabetes mellitus and the underlying mechanisms: a review. *Front Pharmacol*. 2019;10:805. doi:10.3389/fphar.2019.00805
39. Golubev D, Zemskaya N, Shevchenko O, et al. Honeysuckle extract (Lonicera pallasii L.) exerts antioxidant properties and extends the lifespan and healthspan of Drosophila melanogaster. *Biogerontology*. 2022;23(2):215–235. doi:10.1007/s10522-022-09954-1
40. Sze SC, Tong Y, Ng TB, Cheng CL, Cheung HP. Herba Epimedii: anti-oxidative properties and its medical implications. *Molecules*. 2010;15 (11):7861–7870. doi:10.3390/molecules15117861
41. Huo W, Li H, Li L, et al. [Study on regulation of CYP450 enzyme system to reduce liver toxicity through compatibility of Aconiti Kusnezoffii Radix Cocta with Chebulae Fructus and Glycyrrhizae Radix et Rhizoma]. *Zhongguo Zhong yao za zhi*. 2022;47(6):1618–1624. Catalan. doi:10.19540/j.cnki.cjcmm.20211210.403
42. Imran M, Rauf A, Abu-Izneid T, et al. Luteolin, a flavonoid, as an anticancer agent: a review. *Biomed Pharmacother*. 2019;112:108612. doi:10.1016/j.biopha.2019.108612
43. Si H, Wyeth RP, Liu D. The flavonoid luteolin induces nitric oxide production and arterial relaxation. *Eur J Nutr*. 2014;53(1):269–275. doi:10.1007/s00394-013-0525-7
44. Yang W, Li Q, Duncan JW, et al. Luteolin-induced vasorelaxation in uterine arteries from normal pregnant rats. *Pregnancy Hypertens*. 2021;23:11–17. doi:10.1016/j.preghy.2020.10.008
45. El-Bassossy HM, Abo-Warda SM, Fahmy A. Chrysin and luteolin attenuate diabetes-induced impairment in endothelial-dependent relaxation: effect on lipid profile, AGEs and NO generation. *Phytother Res*. 2013;27(11):1678–1684. doi:10.1002/ptr.4917
46. Yao X, Jiang W, Yu D, Yan Z. Luteolin inhibits proliferation and induces apoptosis of human melanoma cells in vivo and in vitro by suppressing MMP-2 and MMP-9 through the PI3K/AKT pathway. *Food Funct*. 2019;10(2):703–712. doi:10.1039/c8fo02013b
47. Zhang D, Li Y, Jiang W, Li W, Yuan X, Lin Z. A network pharmacology-based treatment analysis of luteolin for regulating pyroptosis in acute lung injury. *Shock*. 2023;60(2):306–314. doi:10.1097/shk.0000000000002168
48. Takamiya Y, Fukami K, Yamagishi S, et al. Experimental diabetic nephropathy is accelerated in matrix metalloproteinase-2 knockout mice. *Nephrol Dial Transplant*. 2013;28(1):55–62. doi:10.1093/ndt/gfs387
49. Gwinn DM, Lee AG, Briones-Martin-Del-Campo M, et al. Oncogenic KRAS regulates amino acid homeostasis and asparagine biosynthesis via ATF4 and alters sensitivity to L-Asparaginase. *Cancer Cell*. 2018;33(1):91–107.e6. doi:10.1016/j.ccell.2017.12.003
50. Li J, Davidson D, Martins Souza C, et al. Loss of PTPN12 stimulates progression of ErbB2-dependent breast cancer by enhancing cell survival, migration, and epithelial-to-mesenchymal transition. *Mol Cell Biol*. 2015;35(23):4069–4082. doi:10.1128/mcb.00741-15
51. Li X, Kumar A, Carmeliet P. Metabolic Pathways Fueling the Endothelial Cell Drive. *Annu Rev Physiol*. 2019;81:483–503. doi:10.1146/annurev-physiol-020518-114731
52. Lin Q, Wang H, Lin X, Zhang W, Huang S, Zheng Y. PTPN12 affects nasopharyngeal carcinoma cell proliferation and migration through regulating EGFR. *Cancer Biother Radiopharm*. 2018;33(2):60–64. doi:10.1089/cbr.2017.2254
53. Wang Z, Jiang L, Wang J, Chai Z, Xiong W. Morphine promotes angiogenesis by activating PI3K/Akt/HIF-1α pathway and upregulating VEGF in hepatocellular carcinoma. *J Gastrointest Oncol*. 2021;12(4):1761–1772. doi:10.21037/jgo-20-394

54. Xing L, Chen Y, He Z, et al. Acupuncture improves endometrial angiogenesis by activating PI3K/AKT pathway in a rat model with PCOS. *Evid Based Complement Alternat Med*. 2022;2022:1790041. doi:10.1155/2022/1790041
55. Zheng C, Toth J, Bigwarfe T, et al. Non-neutralizing antibodies increase endogenous circulating Ang1 levels. *mAbs*. 2018;10(8):1260–1268. doi:10.1080/19420862.2018.1521130
56. El-Mas MM, Fan M, Abdel-Rahman AA. Facilitation of myocardial PI3K/Akt/nNOS signaling contributes to ethanol-evoked hypotension in female rats. *Alcohol Clin Exp Res*. 2009;33(7):1158–1168. doi:10.1111/j.1530-0277.2009.00939.x
57. Gingerich S, Krukoff TL. Activation of ERbeta increases levels of phosphorylated nNOS and NO production through a Src/PI3K/Akt-dependent pathway in hypothalamic neurons. *Neuropharmacology*. 2008;55(5):878–885. doi:10.1016/j.neuropharm.2008.06.058